HYPERSPECTRAL CLOUD SHADOW REMOVAL BASED ON LINEAR UNMIXING

Yi Liu [a], José Bioucas-Dias [b], Jun Li [c], Antonio Plaza [a]

[a]Dept. of Technol. of Comput. & Commun., Univ. of Extremadura, Cáceres, Spain (e-mail: {yiliu, aplaza}@unex.es)
[b]Instituto de Telecomunicações, Instituto Superior Técnico Universidade de Lisboa, Lisboa, Portugal (e-mail: bioucas@lx.it.pt)
[c]School of Geography and Planning, Sun Yat-sen University, Guangzhou, China (e-mail: lijun48@mail.sysu.edu.cn).

ABSTRACT

This work introduces a cloud shadow removal method for hyperspectral images (HSIs) based on hyperspectral unmixing. The shading is modeled by a spectral offset and a spectral-dependent attenuation. The offset and the attenuation are estimated by solving a nonconvex optimization problem, which exploits the linear mixing model (LMM). The mixing matrix of the LMM is estimated from the unshadowed image areas. The effectiveness of the proposed method is assessed from classification results of the Houston 2013 (Compact Airborne Spectrographic Imager (CASI) spectrometer VHR HS), whose shadowed areas were removed with the proposed method. The obtained results indicate classification performances in the shadowed areas very close to those of the unshadowed ones, thus providing evidence of the effectiveness of the proposed shading removal technique.

Index Terms— Cloud shadow removal, linear unmixing, HSI, alternating optimization, classification.

1. INTRODUCTION

Clouds have been a significant concern for remote sensing imaging and analysis in the context of land surface monitoring, object detection, quantitative retrieval etc [2]. Although the airborne instruments usually fly below clouds, some pixels still suffer from distorted spectral signatures due to the imbalanced sun illumination. As a result, the spectral signature inconsistency between shadowed and well-illuminated pixels amounts to huge challenges for remote sensing image analysis.

In order to handle this problem, many models and techniques have been developed [3, 4]. A standard paradigm for deshadowing is based on the linear mixture model (LMM), which physically interprets all object signatures as fractions of spectral endmembers associated with specific materials. In the work [5], the authors attacked this problem by conducting linear spectral unmixing twice in both shadowed and unshadowed areas, followed by an endmember matching algorithm that searches and builds the mapping relationship between the shadowed and unshadowed endmembers. Similarly, another effort adopted the same approach but presenting a new endmember matching algorithm in polar coordinates[1]. Both algorithms, when performed twice, tends to produce inconsistencies between the two groups of endmembers due to, namely, the lack of consistency of the unmixing results.

Feature transformations such as principal component analysis (PCA) [6] or kernel manifold alignment (KEMA) [1] have also been exploited to address this shadowing problem. In both methods, [6] and [1], two groups of extracted features are simultaneously obtained and then used to build a mapping relationship. The original physical information, however, is often missing after the feature transformation. Other techniques and algorithms have also been developed to deal with this issue, such as the matched filtering (MF) method [7] and methods based on atmospheric correction [8]. However, uncertainties and model mismatches may also be observed in these cases. When the objective is image classification, the often large quantization errors observed in signatures of shadowed pixels may impair the endmember/feature extraction step. In addition, the limited availability of labeled references (especially for hyperspectral images) also limits the application of supervised techniques.

Motivated by the aforementioned shortcomings of the shadow removal techniques, the contributions in this work are the following: 1) a wavelength dependent affine model for the shadowing process; 2) an LMM unmixed based cloud shadow removal method, where the unmixing is conducted only in the unshadowed areas, thus avoiding hurdles linked with poor quantization of the shadowed pixels; 3) experimental evaluation of the proposed method in an HSI classification problem.

The paper is organized as follows. The proposed shadowing model and shadow removal method are introduced in Section 2. The experimental evaluation in a classification scenario is conducted in Section 3. Finally, Section 4 concludes the paper with a few concluding remarks and future perspectives.

Thanks to (China Scholarship Council) CSC agency for funding. This work has been supported by Junta de Extremadura (decreto 297/2014, ayudas para la realizacin de actividades de investigacin y desarrollo tecnolgico, de divulgacin y de transferencia de conocimiento por los Grupos de Investigacin de Extremadura, Ref. GR15005) and by Portuguese Fundao para a Cilncia e Tecnologia (FCT) under the grants UID/EEA/5008/2013 and ERANETMED/0001/2014.

[1]http://spie.org/newsroom/1209-removing-shadows-from-hyperspectral-images-leaves-nowhere-to-hide

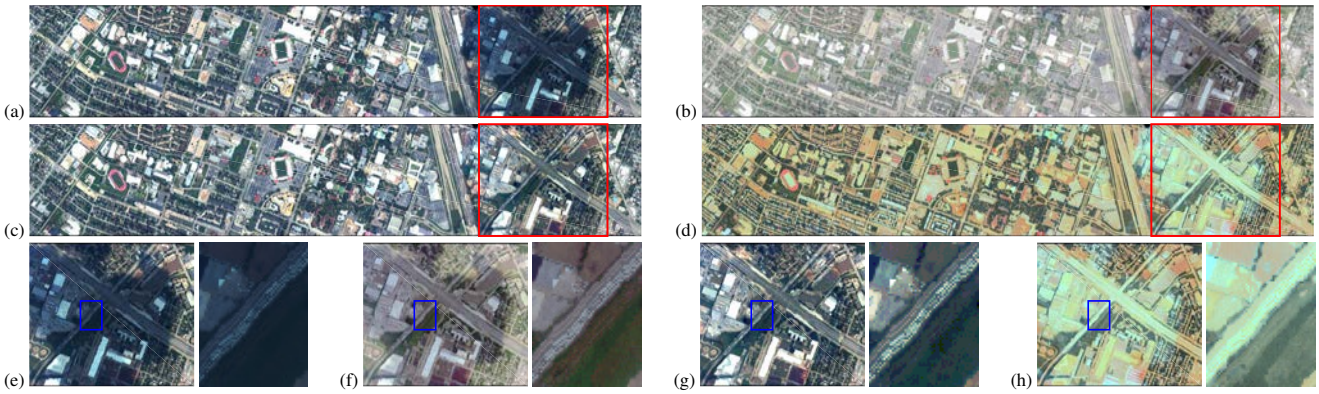

Fig. 1. Houston dataset used in the IEEE GRSS Data Fusion Contest 2013 with: (a) original RGB composite, (b) square-root brightened RGB composite of (a) with (a)'s red window clip (e), and (c, d) the RGB composites that are recovered by the (local histogram matching method) LHM [1] and the proposed method, respectively. Similarly, (e,f,g,h) are corresponding clips in the red windows of (a,b,c,d), respectively, along with their zoomed clips in the blue windows.

2. METHODOLOGIES

2.1. LMM-based shadowing model

Let $\mathbf{Y} \equiv [\mathbf{y}_1, \ldots, \mathbf{y}_n] \in \mathbb{R}^{d\times n}$ be the matrix representation of an hyperspectral image with n spatial samples and d spectral bands. We assume that the observed spectral vectors are well approximated by the LMM [9]. This is

$$\begin{aligned} &\mathbf{Y} = \mathbf{X}\mathbf{Z} + \mathbf{N} \\ &\text{s.t.}: \quad \mathbf{Z} \geq 0,\ \mathbf{1}_p^T\mathbf{Z} = \mathbf{1}_n^T, \end{aligned} \tag{1}$$

where $\mathbf{X} \equiv [\mathbf{x}_1, \ldots, \mathbf{x}_p] \in \mathbb{R}^{d\times p}$ is a mixing matrix containing p endmembers with $\mathbf{x}_i$ representing the i-th endmember signatures, $\mathbf{Z} \equiv [\mathbf{z}_1, \ldots, \mathbf{z}_n] \in \mathbb{R}^{p\times n}$ denotes the abundance matrix, comprising of the endmember fractions $\mathbf{z}_i$, for $i = 1, \cdots, n$, $\mathbf{1}_p = [1, 1, \cdots, 1]^T$, and the constraints represents, respectively, the abundance nonnegativity constraint and the sum-to-one constraint. In addition, $\mathbf{N}$ is a matrix of errors that may influence the data measure process (e.g., noise). The pixel $\mathbf{y}_i$ can, thus, be interpreted as the linear combination of the endmember signatures $\mathbf{x}_i$ with weights (i.e., abundances) $\mathbf{z}_i$.

We assume the following model for a shadowed pixel $\mathbf{y}_s$:

$$\mathbf{y}_s = \boldsymbol{\alpha} + \mathbf{C}\mathbf{y}, \tag{2}$$

where $\mathbf{y}$ is the unshadowed reflectance, $\boldsymbol{\alpha} \equiv [\alpha_1, \cdots, \alpha_d]^T$ is a pixel independent offset vector, and $\mathbf{C} \equiv \text{diag}\{c_1, \cdots, c_d\}$ is diagonal matrix accounting for the wavelength dependent attenuation. Thus, having into consideration the LMM, the reflectance of the m shadowed pixels $\mathbf{Y}_s = [\mathbf{y}_{1,s}, \ldots, \mathbf{y}_{m,s}]$, affected by a given shadow, is given by

$$\begin{aligned} &\mathbf{Y}_s = (\boldsymbol{\alpha}\mathbf{h}^T + \mathbf{C}\mathbf{X})\mathbf{Z} + \mathbf{N}_s \\ &\text{s.t.}: \quad \mathbf{Z} \geq 0,\ \mathbf{1}_p^T\mathbf{Z} = \mathbf{1}_m^T, \end{aligned} \tag{3}$$

where $\mathbf{h}^{p\times 1} = [1, ..., 1]^T$ is a vector of p 1s and $\mathbf{N}_s$ denotes the noise matrix associated with the shadowed pixels.

Algorithm 1: Estimation of cloud shadowing parameters

Input: $\mathbf{Y}_s \in \mathbb{R}^{d\times m}$; `// shadowed spectral vectors`
Input: $\mathbf{X} \in \mathbb{R}^{d\times p}$; `// endmember signatures`
Input: $\mathbf{h} = \mathbf{1} \in \mathbb{R}^{p\times 1}$; `// column 1-vector`
Input: E_{thr}; `// threshold residual`
Output: $\widehat{\mathbf{Z}}, \widehat{\mathbf{C}}, \widehat{\boldsymbol{\alpha}}$; `// variables to estimate`

Initialization: $i = 0$, $E = \infty$, $\widehat{\mathbf{M}} = \mathbf{X}$, $\widehat{\mathbf{C}} = \mathbf{I}$, $\widehat{\boldsymbol{\alpha}} = \mathbf{0}$
while $i < i_{max}$ *or* $E \leq E_{thr}$ **do**
  step 1. Estimate $\widehat{\mathbf{Z}}$:
    $\widehat{\mathbf{Z}} := \arg\min_{\mathbf{Z}} (1/2)||\widehat{\mathbf{M}}\mathbf{Z} - \mathbf{Y}_s||_F^2$;
    s.t.: $\mathbf{Z} \geq 0,\ \mathbf{1}_p^T\mathbf{Z} = \mathbf{1}_m^T$
  step 2. Estimate $\widehat{\boldsymbol{\alpha}}$:
    $\widehat{\boldsymbol{\alpha}} := (\mathbf{Y}_s - \widehat{\mathbf{C}}\mathbf{X}\widehat{\mathbf{Z}})\widehat{\mathbf{Z}}^T\mathbf{h}(\mathbf{h}^T\widehat{\mathbf{Z}}\widehat{\mathbf{Z}}^T\mathbf{h})^{-1}$;
  step 3. Given $\widehat{\mathbf{A}} = \mathbf{Y}_s - \widehat{\boldsymbol{\alpha}}\mathbf{h}^T\widehat{\mathbf{Z}}$, $\widehat{\mathbf{B}} = \mathbf{X}\widehat{\mathbf{Z}}$, estimate $\widehat{\mathbf{C}}$
    $\widehat{c}_j := \frac{\widehat{\mathbf{A}}_{[i]}\widehat{\mathbf{B}}_{[i]}^T}{||\widehat{\mathbf{B}}_{[i]}||_2^2}$, for $j \in \{1, \cdots, d\}$;
    $\widehat{\mathbf{M}} := \widehat{\boldsymbol{\alpha}}\mathbf{h}^T + \widehat{\mathbf{C}}\mathbf{X}$;
    $E := ||\mathbf{Y}_s - \widehat{\mathbf{M}}\widehat{\mathbf{Z}}||_F^2$;
    $i = i + 1$; `// stop flags`
end

In model (3), $\mathbf{Z}$ is the abundance fraction matrix, and $\mathbf{X}$ represents mixing matrix of the unshadowed pixels. Hence, $\mathbf{M} \equiv (\boldsymbol{\alpha}\mathbf{h}^T + \mathbf{C}\mathbf{X})$ can be interpreted as the mixing matrix of an LMM describing the shadowed pixels. Accordingly, we term $\mathbf{M}$ the the shadowed endmember matrix.

2.2. Estimation of the shadowing model parameters

Given the shadowed spectral vectors $\mathbf{Y}_s$ and the mixing matrix $\mathbf{X}$, which was previously estimated from the unshadowed pixels, using, from example, an endmember extraction algorithm, the spectral offset $\boldsymbol{\alpha}$, the attenuation matrix $\mathbf{C}$, and the abundance vector $\mathbf{Z}$ are estimated by solving the nonconvex

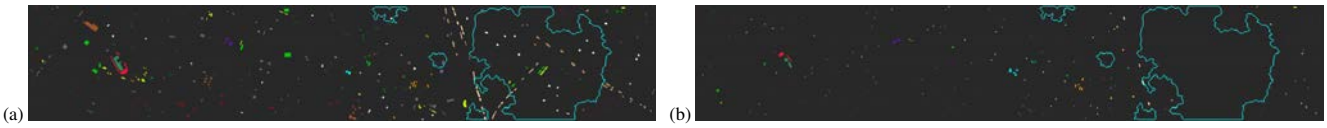

Fig. 2. (a) Test(12197) and (b) training(2832) labels. The shadow areas are obtained by morphological operators.

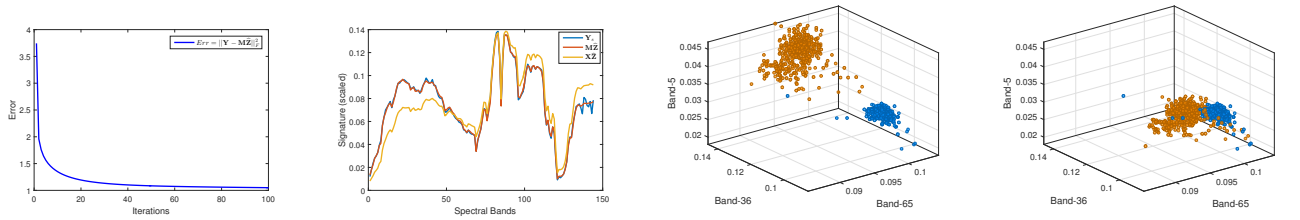

(a) Error (b) Pixel signature (scaled) (c) Scatering before our method (d) Scatering after our method

Fig. 3. (a) plots the object function values in 100 iterations. (b) shows the relevant variables with $\mathbf{Y}_s$: the shaded signature at(1637, 90), $\mathbf{M}\widehat{\mathbf{Z}}$: $\mathbf{Y}_s$'s estimation and $\mathbf{X}\widehat{\mathbf{Z}}$: the recovered signature. (c) scatters samples of the same class inside (orange points) and outside (blue points) the shadow, while (d) scatters the recovered result by the proposed method.

optimization

$$(\widehat{\boldsymbol{\alpha}}, \widehat{\mathbf{C}}, \widehat{\mathbf{Z}}) \in \arg \min_{\boldsymbol{\alpha},\mathbf{C},\mathbf{Z}} (1/2)||(\boldsymbol{\alpha}\mathbf{h}^T + \mathbf{C}\mathbf{X})\mathbf{Z} - \mathbf{Y}_s||_F^2,$$
$$\text{s.t.}: \quad \mathbf{Z} \geq 0, \ \mathbf{1}_p^T\mathbf{Z} = \mathbf{1}_m^T. \tag{4}$$

Optimization (4) is nonconvex that is thus hard to solve. Algorithm 1 implements alternating optimization to compute a local minimum of (4). The optimization in lines 4 and 5 is a *fully constraint least square* (FCLS) problem, which can be solved by the (*Spectral UNmixing by Splitting and Augmented Lagrangian*) SUnSAL algorithm [10]. The solution of (4) with respect to the offset vector $\widehat{\boldsymbol{\alpha}}$, which is a quadratic optimization, is shown in line 7. The solution of (4) with respect to the diagonal attenuation matrix $\mathbf{C}$, which is also a quadratic optimization, is shown in line 9.

To conclude the cloud removal procedure, we compute the unshadowed spectral vectors as

$$\mathbf{Y} = \mathbf{X}\widehat{\mathbf{Z}}. \tag{5}$$

The shadow removal performance of the proposed method can be perceived in Fig. 3 (b) showing a close description of the estimated variables to the real ones. This observation can be further supported by comparing the scattering plots in Fig. 3 (c,d). And besides, the plot in Fig. 3 (a) indicates the convergence of the object function (4) provided by our method Algorithm 1 along 100 iterations.

3. EXPERIMETAL RESULTS

3.1. Experimental data and setup

In this section, we evaluate the performance of the proposed method using a hyperspectral data set obtained by the Compact Airborne Spectrographic Imager (CASI) spectrometer and an aerial LiDAR data set collected over the city of Houston in 2013 [2] (see Fig. 1). The HSI data size is 349(lines)×1905(columns)×144(bands) acquired in the wavelength interval ranging from 380 nm to 1050 nm, with the samples collected in Fig. 2. To start with, this image data used in our case have been transformed by the perspective projection [11, 9] to the mean spectral vectors of the original data, in order to enforce the transformed spectral vectors in the same affine space. We test the proposed method in a classification problem, using the MLR-LORSAL [12] classifier without training samples inside of the shadow area. And in a way similarly to the work [13], we use the Markov random fields (MFRs) with the classification result provided by MLR-LORSAL in order to promote the spatial smoothness. In addition, the unsupervised local histogram matching (LHM) method [1] has also been employed for comparison purposes.

3.2. Shadow removal and classification performance

As shown in Fig. 1, the proposed method, with clearer object textures and distinct local contrast especially with respect to different types of plants (in the blue windows), outperforms the LHM method. This is due to that our method reconstructs the shadowed pixels considering both the shadowed signatures and unshadowed endmembers (see (5) and line 4 of Algorithm 1), whereas the LHM method only relies on the histogram structures in the lack of physical meaning. Meanwhile, our results show lower inaccuracies in shadow boundaries caused by cloud edges.

In the following, we conduct a classification experiment to further evaluate the capacity of our proposed method to improve the generalization ability of a classifier. In this case, the classifier is trained with samples only from the cloud-shadow-

[2] http www.grss-ieee.orgcommunitytechnical-committeesdata-fusion2013-ieee-grss-data-fusion-contest

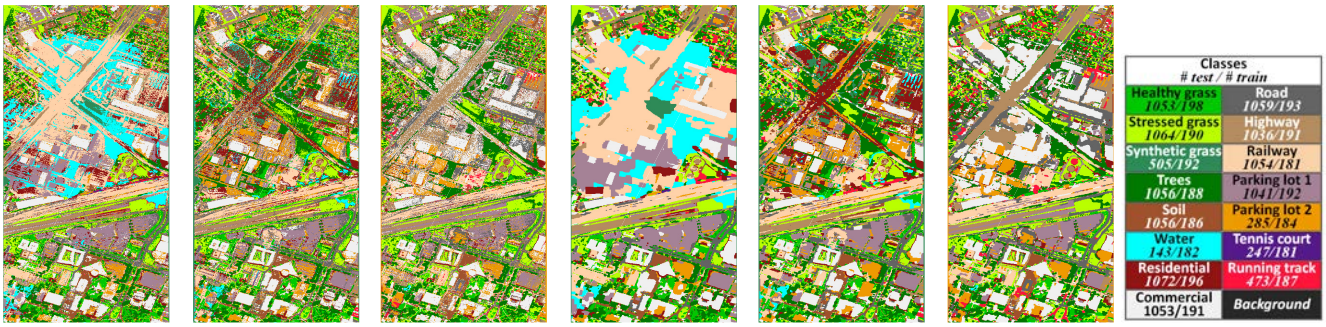

(a) 81.01% / 33.17% (b) 82.99% / 39.35% (c) **85.23% / 58.74%** (d) 83.23% / 26.12% (e) 85.21% / 38.91% (f) **90.38% / 59.85%** (g) Legend

Fig. 4. Classification maps of the shadow areas by different classification methods, MLR-LORSAL (a-c) and MLR-LORSAL-MRF (d-f), respectively, with the input of the original data(a,d), results by LHM method(b,e) and results by the proposed method(c,f). The values #%/#% denotes the overall accuracies (OA), respectively, for the whole test samples and the shadowed test samples.

free areas, and then tested with samples from both the cloud shadowed and unshadowed areas. In Fig. 4, the classification results with different inputs (the data of the original, the LHM method, and the proposed method) have been displayed, both considering only spectral information (MLR-LORSAL) and spatial+spectral information (MLR-LORSAL-MRF), respectively. From Fig. 4, we can observe that our proposed method outperforms the LHM according to the test samples both inside and outside of the shadow areas. Especially for the samples inside of the shadow areas, our proposed method remarkably increases the overall accuracies (OA) by 25.57% (compared with only using the original image) and by 19.39% (compared with the LHM method). With the inclusion of spatial information by means of the MRF, the OA achieved by our method reaches 90.38% and 59.85%, respectively, for samples that are outside of and inside of the shadow areas. Also illustratively, our proposed method acquires more satisfactory classification maps when compared to other methods.

4. CONCLUSIONS

This paper proposed a new cloud-shadow removal method for hyperspectral images that can deal with the inconsistencies in the pixel signatures caused by cloud shadows that may appear in a classification problem. A feasible solution is provided based on the application of linear spectral unmixing. Our proposed method just needs to apply the spectral unmixing step once, instead of twice as other widely used methods. In this way, the proposed model avoids possible inconsistencies and uncertainties resulted from the application of unmixing separately on shadow and nonshadow pixels. The performance of the method, evaluated in the context of a classification scenario with partially shadowed HSI data, indicates that our approach is capable of bridging and dealing with the differences between the shadowed and well-illuminated pixels and thus promoting the generalizing ability of a classifier. Future work will further consider the thickness of the cloud and also focus on exploring its potential in multi-sensor and multi-temporal remote sensing image data analysis.

5. REFERENCES

[1] D. Tuia, D. Marcos, and G. Camps-Valls, "Multi-temporal and multi-source remote sensing image classification by nonlinear relative normalization," *ISPRS*, vol. 120, pp. 1–12, 2016.

[2] J. Bioucas-Dias, A. Plaza, G. Camps-Valls, et al., "Hyperspectral remote sensing data analysis and future challenges," *EEE Geosci. Remote Sens. Mag*, vol. 1, no. 2, pp. 6–36, 2013.

[3] D. Rüfenacht, C. Fredembach, and S. Süsstrunk, "Automatic and accurate shadow detection using near-infrared information," *IEEE Trans. Pattern Anal. Mach. Intell.*, vol. 36, no. 8, pp. 1672–1678, 2014.

[4] R. Richter and A. Müller, "De-shadowing of satellite/airborne imagery," *Int. J. Remote Sens.*, vol. 26, no. 15, pp. 3137–3148, 2005.

[5] F. Omruuzun, D. Baskurt, H. Daglayan, et al., "Shadow removal from vnir hyperspectral remote sensing imagery with endmember signature analysis," in *SPIE Sensing Technology + Applications*. International Society for Optics and Photonics, 2015, pp. 94821F–94821F.

[6] T. Mori, R. Taketa, S. Hiura, et al., "Photometric linearization by robust pca for shadow and specular removal," in *Computer Vision, Imaging and Computer Graphics. Theory and Application*, pp. 211–224. Springer, 2013.

[7] T. Roper and M. Andrews, "Shadow modelling and correction techniques in hyperspectral imaging," *Electronics Letters*, vol. 49, no. 7, pp. 458–460, 2013.

[8] M. Matthew, S. Adler-Golden, A. Berk, et al., "Status of atmospheric correction using a modtran4-based algorithm," in *AeroSense 2000*. International Society for Optics and Photonics, 2000, pp. 199–207.

[9] J. Bioucas-Dias, A. Plaza, N. Dobigeon, et al., "Hyperspectral unmixing overview: Geometrical, statistical, and sparse regression-based approaches," *IEEE J. Sel. Topics Appl. Earth Observ. in Remote Sens.*, vol. 5, no. 2, pp. 354–379, 2012.

[10] J. Bioucas-Dias and M. Figueiredo, "Alternating direction algorithms for constrained sparse regression: Application to hyperspectral unmixing," in *2nd WHISPERS'2010*. IEEE, 2010, pp. 1–4.

[11] M. Craig, "Minimum-volume transforms for remotely sensed data," *IEEE Trans. Geosci. Remote Sens.*, vol. 32, no. 3, pp. 542–552, 1994.

[12] J. Bioucas-Dias and M. Figueered, "Logistic regression via variable splitting and augmented lagrangian tools," Tech. Rep., Instituto Superior Tecnico, TULisbon, 2009.

[13] J. Li, J. Bioucas-Dias, and A. Plaza, "Spectral–spatial hyperspectral image segmentation using subspace multinomial logistic regression and markov random fields," *IEEE Trans. Geosci. Remote Sens.*, vol. 50, no. 3, pp. 809–823, 2012.